IEEE Journal of Microwaves

Received 11 April 2023; revised 24 May 2023 and 11 June 2023; accepted 6 July 2023. Date of publication 31 July 2023; date of current version 9 October 2023.

*Digital Object Identifier 10.1109/JMW.2023.3294106*

# Optimal Adjacent Output Phase Difference Assignments in One-Dimensional Parallel Switching Matrices With Four Beams

**SHENGJIA WU [1] (Student Member, IEEE), JIRO HIROKAWA [1] (Fellow, IEEE), TAKASHI TOMURA [1] (Member, IEEE), AND NELSON J. G. FONSECA [2] (Senior Member, IEEE)**

*(Regular Paper)*

[1]Department of Electrical and Electronic Engineering, Tokyo Institute of Technology, Tokyo 152-8552, Japan
[2]Antennas and Sub-Millimetre Waves Section, European Space Agency, NL-2200 AG Noordwijk, The Netherlands

CORRESPONDING AUTHOR: Jiro Hirokawa (e-mail: jiro@ee.e.titech.ac.jp).

This work was supported by SCOPE under Grant JP215004001 of the Ministry of Internal Affairs and Communications, Japan.

**ABSTRACT** This article provides for the first time a detailed discussion of the optimal assignment of adjacent output phase differences in terms of matrix performance out of all possible combinations in generalized one-dimensional parallel switching matrices with four beams. In this specific case, the topology of the proposed matrix reduces to that of a single-layer Butler matrix, connecting hybrid couplers and crossovers with adequate phase shifters. The values of the phase shift required are dependent on the assignment of the output phase differences, which in turn is shown to have an impact on the radiation characteristics of the linear array fed by such networks when imposing constraints on the matrix layout for a more generic implementation. The configuration having the smallest phase difference with reference to the transmission phase of a straight waveguide with the same length as the coupled region of the crossover is chosen and compared with the conventional well-known Butler matrix. The two matrix configurations are implemented using post-wall waveguides designed to operate over the band 20 GHz – 24 GHz. The prototypes are manufactured and tested, using transitions to standard waveguide WR42. The measured results confirm the benefits of the identified optimal adjacent phase difference assignment in terms of transmission coefficients, reflection coefficients, phase differences between adjacent output ports, and frequency dependence of the array factor. These results will also benefit the design of larger generalized one-dimensional parallel switching matrices.

**INDEX TERMS** Beam switching, Butler matrix, cross junction, hybrid coupler, Nolen matrix, waveguide short-slot-coupler.

## I. INTRODUCTION

Agile antennas are an essential component of modern-day wireless communication networks. While electronically steerable antenna technologies have made significant progress over recent years [1], their cost and power consumption remain major limitations for several applications, such as mobile systems and battery-powered sensors. Beamforming networks (BFNs) are a convenient alternative to realize low-cost analogue multiple beam antenna arrays making use of mass-production printed circuit board (PCB) techniques [2]. Although introduced more than half a century ago, BFN design is still a very active field of research, particularly in the space sector where they are being developed for both the space and ground segments [3], [4]. There are several well-known BFNs, including the Blass matrix [5], [6], the Butler matrix [7], [8], [9], [10], and the Nolen matrix [11], [12], [13], which enable to produce multiple simultaneous beams over a wide angular range.

The Blass matrix is the most flexible design but has generally higher power loss due to loads in the structure; while the Butler matrix is canonically lossless but has less flexibility in the multiple beam distribution [14]. The Nolen matrix is a generalized form of lossless beamforming network which combines some of the advantages of the Blass and Butler matrices [15]. Nevertheless, the Butler matrix and the Nolen matrix have shortcomings as well. The Nolen matrix can have an arbitrary number of beams, while the number of beams that the Butler matrix can generate is limited to a power of two. A variant of Butler matrices using 3×3 BFNs as building blocks was also proposed [16] and recently demonstrated experimentally [17], but this configuration constrains the number of beams to a power of three. The Butler matrix is equivalent to the fast Fourier transform [18], [19] and has the least number of components for a theoretically lossless matrix. This results in crossovers between transmission lines, generally implemented using a two-layer design but resulting in a more complex implementation in single-layer PCB designs. The Nolen matrix has no crossovers thanks to its serial configuration. However, there is imbalance between output ports for some of the couplers which can limit the effective bandwidth and requires additional phase corrections combined with a less-compact parallel configuration for a broadband design [20].

General configurations of theoretically lossless one-dimensional parallel switching matrices with an arbitrary number of beams combining most of the advantages discussed above have been proposed recently by some of the authors [21]. These configurations are particularly well suited for low-cost millimeter-wave implementations in a single-layer PCB design using post-wall waveguide technology [22], also known as substrate integrated waveguide [23]. They provide some flexibility in the beam assignments per input ports, characterized by their phase difference between adjacent output ports and corresponding pointing directions, with some specific assignments leading to special matrix configurations as discussed in [24]. The integration of the BFN and linear array benefits from an output port spacing as small as possible to avoid grating lobes, ideally having adjacent ports sharing a common post-wall. Thus, there are obvious advantages in developing a generic matrix design in which parallel paths remain within the envelop of the input and output port layouts so the design may be easily extended to larger matrices. Most Butler matrix designs reported in the literature, which are based on the conventional configuration derived from the fast Fourier transform and associated phase shifter values [7], [18], [19], extend beyond the envelop of the input and output port layouts [25], [26], [27], [28]. The design in [8] is a particular case of a post-wall matrix that remains within the envelop of the input and output port layouts, which obviously constrains the design of the phase shifters. This is expected to have an impact on the BFN performance.

This manuscript provides a detailed comparison of two adjacent output phase difference assignments in 4×4 generalized parallel switching matrices selected as study case. To the best of the authors' knowledge, this is the first time that such a comparison is reported in the literature, highlighting the benefits in implementing the optimal adjacent output phase difference assignment in terms of matrix performance. For this comparison, one assignment has the smallest phase difference with reference to the transmission phase of a straight waveguide with the same length as the coupled region of the crossover. It is selected because it provides the widest fractional bandwidth for some of the key BFN performances such as the array factor obtained with the complex amplitudes at the output ports as well as the reflection and isolation coefficients. The other assignment is the configuration corresponding to the standard 4×4 Butler matrix. Two prototypes are designed and manufactured. The center frequency is 22 GHz, and the frequency bandwidth from 20 GHz to 24 GHz is analyzed. The simulated and measured results of these two assignments are compared.

## II. DESIGN CONSIDERATIONS

Theoretically lossless BFNs impose stringent constraints on the achievable linear array excitations and associated radiation patterns, which are orthogonal [14], [29]. A lossless BFN with dimensions $N \times N$, where $N$ is the number of input ports, also corresponding to the number of beams and number of output ports, produces values of adjacent output phase differences, $p_k$, such that:

$$p_k = \frac{2k\pi}{N} - \frac{(N+1)\pi}{N}, \text{ for } k = 1, \ldots, N \qquad (1)$$

The number of assignments is determined by the permutations of $N$, which is factorial of $N$.

Special assignments of adjacent output phase differences per input ports are discussed in [24]. These are found to result in simplified or peculiar theoretical configurations. A particular case of interest is the configuration comprising two Nolen matrices fed in parallel through hybrid couplers when $N$ is an even number [21]. In this specific case, the number of the output phase difference assignments is $(N/2)!2^{N/2}$. As an example, there are eight special assignments among the total of 24 assignments for $N = 4$ [24]. According to [21], the generalized matrix configuration with four beams is shown as Fig. 1(a).

Using (1), the output phase differences for the specific case $N = 4$ are $-\frac{3}{4}\pi$, $-\frac{1}{4}\pi$, $\frac{1}{4}\pi$, and $\frac{3}{4}\pi$. Eight output phase difference assignments are found to be special since they only require hybrid couplers and crossovers. Consequently, the values in radian of $\theta_1$, $\theta_2$, $\theta_4$, and $\theta_5$ are all $0.25\pi$ for all eight solutions, which means that these four couplers are hybrids. The values of $\theta_3$ and $\theta_6$ are both $0.5\pi$, which are crossovers. Fig. 1(b) shows the configuration for the eight special cases by changing the third and sixth couplers of the general configuration into crossovers. The rest of the couplers are all hybrids. Then the second and fifth phase shifters are moved from the left output port to the right output port of the corresponding coupler, and their values changed from $-\phi_i$ to $+\phi_i$. The modified configuration is shown as Fig. 1(c). It must be noted that the values of phase shifters cannot be uniquely determined in the modified configuration because all paths have at least one phase shifter. To solve this problem, the values of the third and the sixth phase shifters are set equal to zero. By

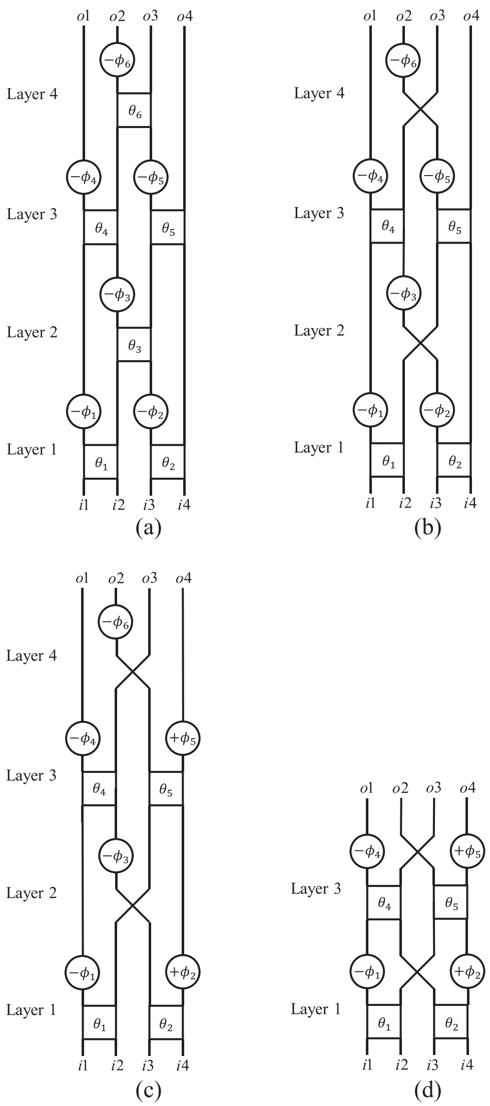


**FIGURE 1.** Configurations of switching matrices with four beams: (a) the general design, (b) the special design, (c) the modified design, and (d) the shortened modified design.

**TABLE 1.** Values of Output Phase Differences Per Input Ports for the Eight Special Assignments in a Switching Matrix With Four Beams

| Assignment | $i_1/\pi$ | $i_2/\pi$ | $i_3/\pi$ | $i_4/\pi$ |
|---|---|---|---|---|
| 1 | −0.75 | 0.25 | −0.25 | 0.75 |
| 2 | −0.75 | 0.25 | 0.75 | −0.25 |
| 3 | 0.25 | −0.75 | −0.25 | 0.75 |
| 4 | 0.25 | −0.75 | 0.75 | −0.25 |
| 5 | −0.25 | 0.75 | −0.75 | 0.25 |
| 6 | −0.25 | 0.75 | 0.25 | −0.75 |
| 7 | 0.75 | −0.25 | −0.75 | 0.25 |
| 8 | 0.75 | −0.25 | 0.25 | −0.75 |

**TABLE 2.** Values of the Phase Shifts for the Eight Special Assignments in a Switching Matrix With Four Beams

| Assignment | $\phi_1/\pi$ | $\phi_2/\pi$ | $\phi_4/\pi$ | $\phi_5/\pi$ |
|---|---|---|---|---|
| 1 | −0.75 | 0.75 | −0.50 | 0.50 |
| 2 | −0.75 | −0.25 | −0.50 | 0.50 |
| 3 | 0.25 | 0.75 | −0.50 | 0.50 |
| 4 | 0.25 | −0.25 | −0.50 | 0.50 |
| 5 | 0.75 | −0.75 | 0.50 | −0.50 |
| 6 | 0.75 | 0.25 | 0.50 | −0.50 |
| 7 | −0.25 | −0.75 | 0.50 | −0.50 |
| 8 | −0.25 | 0.25 | 0.50 | −0.50 |

**TABLE 3.** Values of the Design Parameters of all Couplers (From Center to Center)

| Coupler | $\ell$ (mm) | $w$ (mm) | $d$ (mm) | $d_d$ (mm) | $x_a$ (mm) | $y_a$ (mm) |
|---|---|---|---|---|---|---|
| Hybrid | 10.01 | 13.40 | 3.20 | 2.65 | / | / |
| Crossover 1 | 15.80 | 11.62 | 5.47 | / | 1.10 | 6.60 |
| Crossover 2 | 15.80 | 11.62 | 5.47 | / | 1.25 | 6.40 |
| Crossover 3 | 15.80 | 11.62 | 5.47 | / | 1.21 | 6.30 |
| Crossover 4 | 15.80 | 11.62 | 5.47 | / | 1.29 | 5.96 |

arranging two phase shifters and one crossover in the same row, a compact configuration can be obtained, which is shown as Fig. 1(d). The shortened modified four-beam configuration has the same structure as the conventional Butler matrix, but the values of the phase shifts may differ with the output phase difference assignment. The values of output phase differences per input ports for the eight special assignments are listed in Table 1. Note that Assignment 5 corresponds to the standard Butler matrix configuration, equivalent to the Fast Fourier Transform [7], [20], [21]. Table 2 shows the required values of phase shifts in radian for these eight special assignments. As expected, the special assignments with a symmetric distribution of the phase differences having opposite signs lead to matrices with symmetric phase shifts.

## III. TWO SPECIFIC ASSIGNMENTS IN SHORTENED MODIFIED CONFIGURATION

### A. COUPLER DESIGNS AND ADJUSTED PHASE SHIFT VALUES

The matrices are designed at 22 GHz and implemented on a PTFE substrate having a thickness of 3.2 mm and a dielectric constant of 2.17. Fig. 2(a) shows the basic structure of a coupler using post-wall waveguide technology [26], [27]. The basic structure is used for the design of the hybrid coupler. In the case of the crossover, considering the full structure of the $4 \times 4$ matrix, a phase shifter and a crossover need to share the same post-wall to comply with the imposed constraint on the envelop discussed in the Introduction. Therefore, the design of the crossover is optimized as shown in Fig. 2(b).

Table 3 shows the values of the key design parameters. Both structures have the same broad wall width $a = 7.95$ mm and

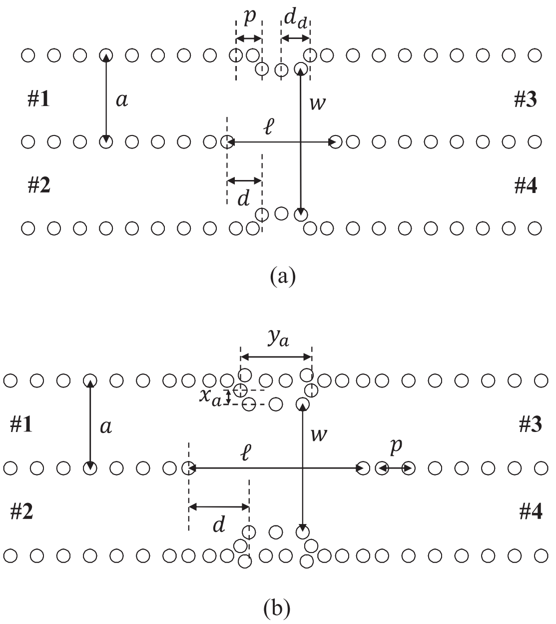


**FIGURE 2.** **Structures and design parameters of (a) the hybrid coupler and (b) the crossover.**

the distance between posts $p = 2.40$ mm. Since the structures of the crossovers have tiny differences according to different phase shifters, four groups of parameters are used. The simulation results of the hybrid and crossover are shown in Fig. 3. The results of the four crossovers are similar so only one result is shown.

According to the simulation results, the reflection coefficient of the hybrid is below −19 dB over a bandwidth of 18.18%, from 20 GHz to 24 GHz. The output port phase difference of the hybrid coupler is −90.43°, −89.97°, and −89.87° at 20 GHz, 22 GHz, and 24 GHz, respectively, compared with the ideal value of −90°. The reflection coefficient of the crossover is below −15 dB over a bandwidth of 11.50%, from 20.92 GHz to 23.45 GHz. The crossover has a transmission phase of 100.66°, corresponding to the coupled region only, deembedding the waveguide ports. Due to the structure of the special configuration with four beams, the values of phase shift need to be adjusted according to the transmission phase of the crossover. After recalculation, the adjusted values of the phase shifts with reference to a straight waveguide having the length of the coupled region of the crossover are obtained for the eight assignments as shown in Table 4.

### B. DESIGN OF PHASE SHIFTERS

Out of the eight special assignments, Assignments 1 and 5 are discussed in this manuscript. Assignment 1 has the smallest phase differences with reference to the transmission phase of a straight waveguide with the same length as the coupled region of the crossover. Each assignment uses two types of phase shifters. Assignment 5 corresponds to the reference standard Butler matrix configuration.

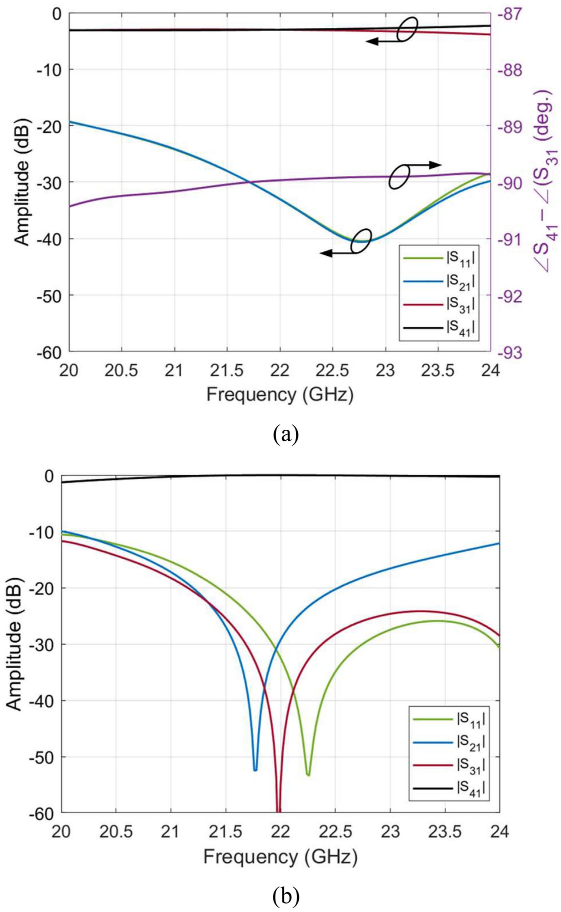


**FIGURE 3.** **Simulation results of the transmission coefficients and the reflection coefficients of (a) the hybrid coupler, including the output port phase difference and (b) the crossover.**

**TABLE 4.** **Adjusted Values of the Phase Shifts for Eight Special Assignments in a Switching Matrix With Four Beams**

| Assignment | $-\phi_1$ (deg.) | $\phi_2$ (deg.) | $-\phi_4$ (deg.) | $\phi_5$ (deg.) |
|---|---|---|---|---|
| 1 | −34.34 | −34.34 | −79.34 | −79.34 |
| 2 | −34.34 | 145.66 | −79.34 | −79.34 |
| 3 | 145.66 | −34.34 | −79.34 | −79.34 |
| 4 | 145.66 | 145.66 | −79.34 | −79.34 |
| 5 | 55.66 | 55.66 | 100.66 | 100.66 |
| 6 | 55.66 | −124.34 | 100.66 | 100.66 |
| 7 | −124.34 | 55.66 | 100.66 | 100.66 |
| 8 | −124.34 | −124.34 | 100.66 | 100.66 |

The phase shift values −34.34° and −79.34° are used for Assignment 1, while the values 55.66° and 100.66° are used for Assignment 5. The post-wall waveguide structure of a phase shifter is shown in Fig. 4. As discussed in the Introduction, the phase shifts are achieved by a reduction of the waveguide cross-section so as not to extend beyond the envelop for each path. By changing the waveguide width and the position of reflection-canceling posts, different phase shift

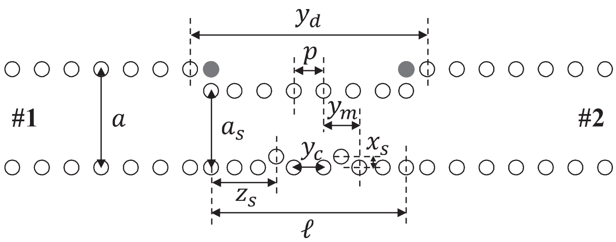


**FIGURE 4.** Structure and design parameters of the phase shifter.

**TABLE 5.** Values of the Design Parameters of the Phase Shifters (From Center to Center)

| Phase Shifter | $a_s$ (mm) | $x_s$ (mm) | $z_s$ (mm) | $y_m$ (mm) | $y_c$ (mm) |
|---|---|---|---|---|---|
| −79.34° | 7.09 | 0.32 | 5.05 | 3.20 | 1.10 |
| −34.34° | 6.76 | 0.50 | 5.10 | 3.20 | 0.90 |
| 55.66° | 6.37 | 0.86 | 5.26 | 3.00 | 1.00 |
| 100.66° | 6.20 | 0.88 | 5.27 | 2.90 | 1.20 |

**TABLE 6.** Frequency Bandwidth With Reflection Below −15 dB for all Phase Shifters

| Phase Shifter | −79.34° | −34.34° | 55.66° | 100.66° |
|---|---|---|---|---|
| Frequency Range (GHz) | 20.00 ~ 23.78 | 20.25 ~ 23.69 | 20.61 ~ 24.00 | 21.23 ~ 24.00 |
| Bandwidth | 17.18% | 15.64% | 15.41% | 12.59% |

values can be achieved. The wider the waveguide width, the smaller the value of phase shift. The structures of the phase shifters are nearly identical, except for the phase shift value 100.66°, which requires two more posts at the two corners (highlighted in grey in Fig. 4). All these structures are symmetrical with reference to the central longitudinal axis. The key design parameters are listed in Table 5. All phase shifters have the same broad wall width $a = 7.95$ mm, distance between posts $p = 2.40$ mm, coupled length $\ell = 15.80$ mm, and $y_d = 19.20$ mm.

The simulated results of the four phase shifters including the transmission coefficients, the reflection coefficients, and the frequency dependence of the phase shift values are reported in Fig. 5. The transmission phase of the crossover is also provided as reference of the phase variation over frequency. According to the results, the bandwidths with reflections below −15 dB for the four phase shifters are listed in Table 6. Over the frequency range from 20 GHz to 24 GHz, the two phase shifters used in Assignment 1 keep large transmission; however, the ones used in Assignment 5 have notable degradation, specifically in the lower range. The reflection of the phase shifter with value 55.66° degrades seriously when the frequency is lower than 20.52 GHz. Similarly, the reflection of the phase shifter with value 100.66° has serious degradation when the frequency is lower than 21.16 GHz. The reason the phase shifters with values 55.66° and 100.66°

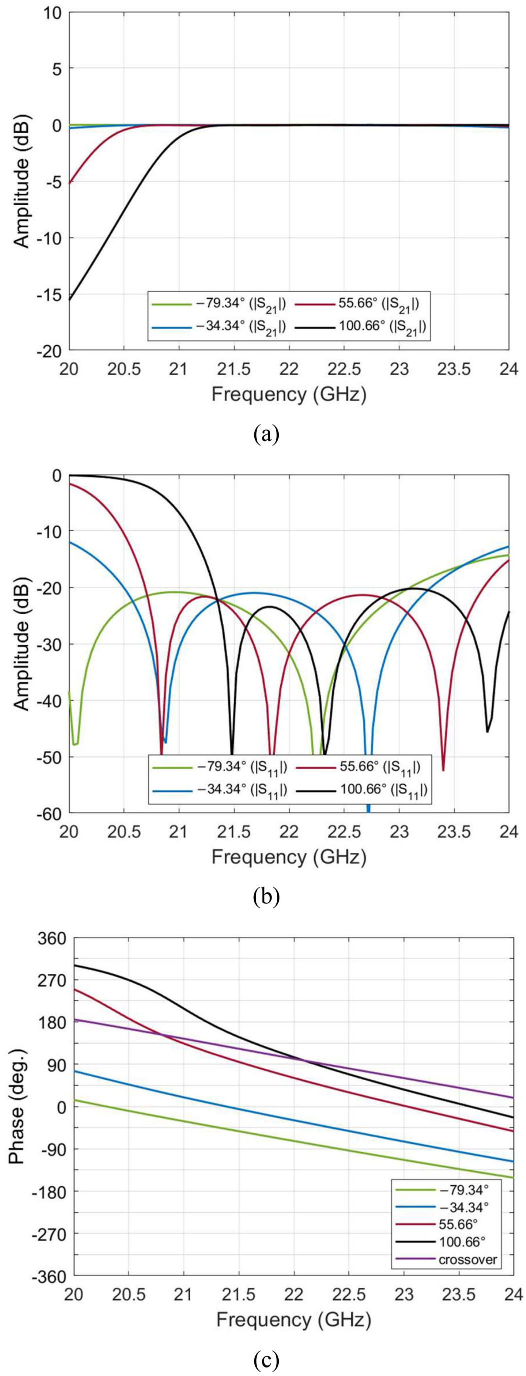


**FIGURE 5.** Simulation results of (a) the transmission coefficients, (b) the reflection coefficients, and (c) the frequency dependence of phase shift values, compared to the transmission phase of the crossover, of the four phase shifters designed.

have narrower bandwidth than −34.34° and −79.34° is that they have larger values of phase shift requiring narrower waveguide width than the other two, leading to higher cut-off frequency. It is also apparent from Fig. 5(c) when comparing the phase variation over frequency of the phase shifters versus the crossover that higher phase error is expected, even within the band with high transmission, for the phase shifters

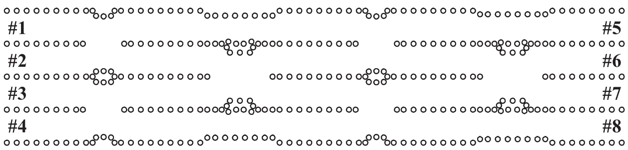


**FIGURE 6.** Structure of a shortened modified 4 × 4 parallel switching matrix design.

with values 55.66° and 100.66°, thus impacting the performance of the matrix not only in the lower frequency range but also in the upper frequency range analyzed. These issues could be circumvented adjusting the design of the phase shifters and/or of the crossover, but this would result in a less compact overall matrix design [25], [26], [27], [28], as discussed in the Introduction. Coincidently, the two phase shifters used in the matrix corresponding to Assignment 1 are the two best designs analyzed, while the two worse designs are both used in the matrix with Assignment 5. These results highlight the importance of output phase difference assignment for optimal performance, further demonstrated in the following section reporting on the performance of the complete matrices.

### *C. DESIGN OF 4 × 4 MATRICES*

Having designed all required components, a full 4 × 4 matrix can be assembled connecting four hybrids, two crossovers, and four phase shifters. Each assignment uses two kinds of phase shifters. As discussed above, Assignment 1 and Assignment 5 have the same structure but use different values of the parameters. The structure of the complete matrix configuration is shown in Fig. 6. The size of both matrices is 148.82 mm × 31.80 mm. Ports 1 to 4 are the input ports, while Ports 5 to 8 are the output ports. Since Assignment 1 and Assignment 5 have symmetrical structures, the two replaced edges should be identical for one crossover. However, if the assignment does not have a symmetrical structure, which means that the values of phase shifters above and below the crossover are not the same, the replaced edges of the crossover would be different. In the case of Assignment 1 and Assignment 5, the structure of the adjusted crossover maintains symmetry. Figs. 7 and 8 report the simulated results of Assignments 1 and 5, respectively. Fig. 7(a) and (b) show the results of Assignment 1 in amplitude for Input ports 1 and 4 and Input ports 2 and 3. For Input ports 1 and 4, the reflection is below −15 dB over a fractional bandwidth of 11.73%, from 20.73 GHz to 23.31 GHz. For Input ports 2 and 3, the reflection is below −15 dB over a bandwidth of 14.77%, from 20.30 GHz to 23.55 GHz. In Fig. 7(a), $S_{41}$ shows a degradation of performance both in the lower and upper frequency range, thus being the limiting parameter for the operating bandwidth. While it is not possible to find a single cause for this reduced bandwidth compared to the other reflection and isolation coefficients of this matrix, which are the consequence of multiple reflections at different levels in the complex component assembly, it is likely driven, due to symmetries, by the isolation of the crossover, having similar bandwidth with a level below −15 dB as shown in Fig. 3(b). Fig. 7(c) reports the phase differences between adjacent output ports. The average phase differences at the center frequency 22 GHz are −134.89°, 44.95°, −44.72°, and 135.12°, which are close to the expected values of −135°, 45°,

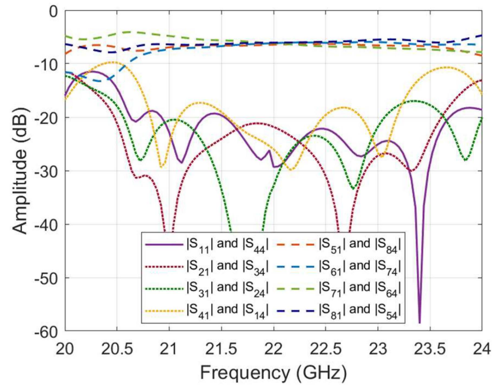


(a)

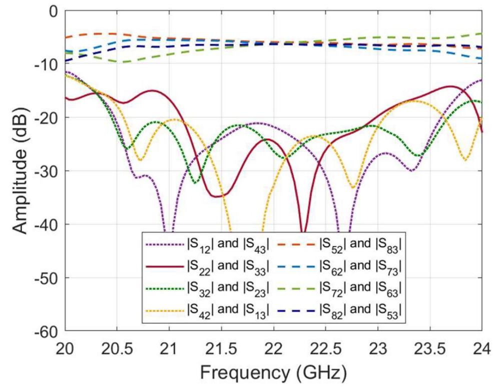


(b)

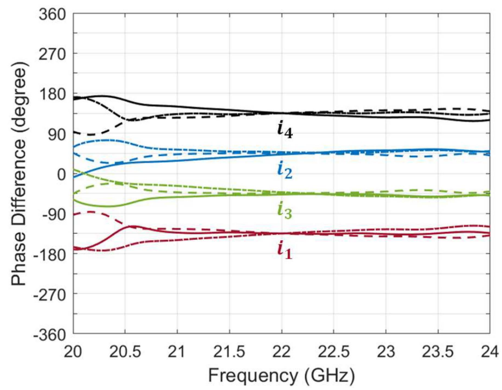


(c)

**FIGURE 7.** Simulation results for assignment 1 of the 4 × 4 parallel switching matrix: (a) and (b) amplitude in dB (reflection coefficients in *solid lines*, port-to-port isolations in *dotted lines*, and transmission coefficients in *dashed lines*), and (c) phase difference between adjacent ports in degree (between port 6 and port 5 in *solid lines*, between port 7 and port 6 in *dashed lines*, and between port 8 and port 7 in *dashed-dotted lines*).

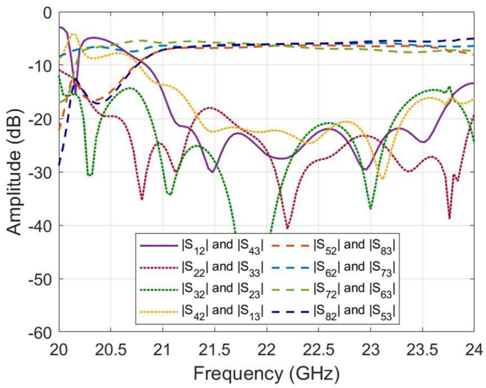


(a)

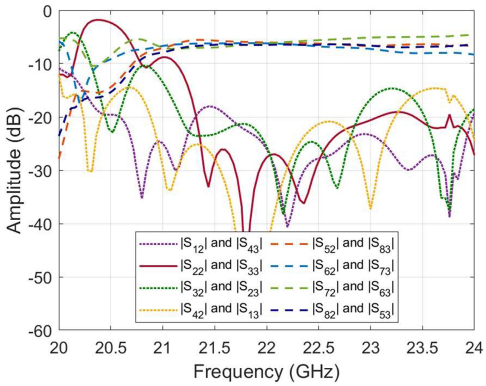


(b)

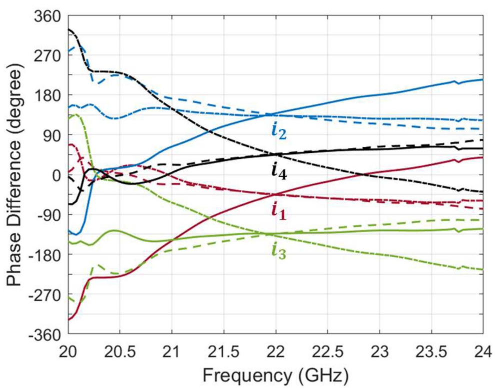


(c)

**FIGURE 8. Simulation results for assignment 5 of the 4 × 4 parallel switching matrix: (a) and (b) amplitude in dB (reflection coefficients in *solid lines*, port-to-port isolations in *dotted lines*, and transmission coefficients in *dashed lines*), and (c) phase difference between adjacent ports in degree (between port 6 and port 5 in *solid lines*, between port 7 and port 6 in *dashed lines*, and between port 8 and port 7 in *dashed-dotted lines*).**

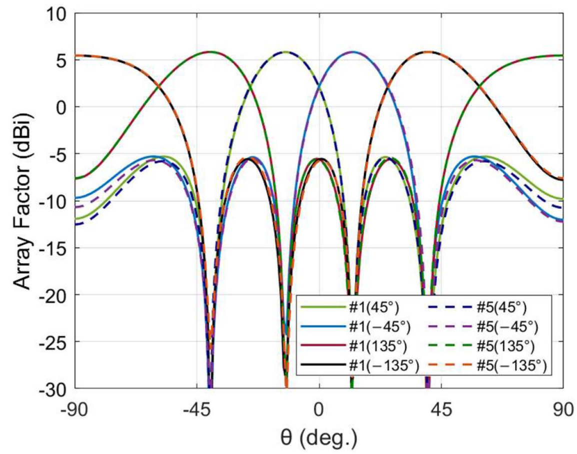


(a)

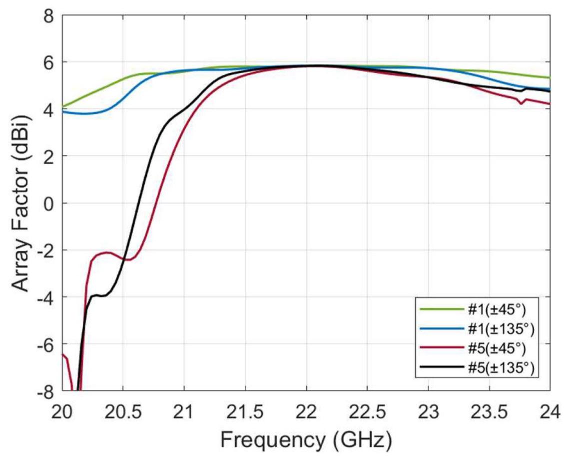


(b)

**FIGURE 9. (a) Array factor pattern at 22 GHz and (b) frequency dependence of the array factor at peak directions for assignments 1 and 5.**

−45°, and 135°. The results for Assignment 5 in amplitude for Input ports 1 and 4 and Input ports 2 and 3 are shown in Fig. 8(a) and (b). Fig. 8(c) shows the phase differences between adjacent output ports. From Fig. 8(a), Input ports 1 and 4 have a reflection below −15 dB over a bandwidth of 10.68%, from 21.16 GHz to 23.51 GHz. From Fig. 8(b), Input ports 2 and 3 have a reflection below −15 dB over a bandwidth of 8.50%, from 21.25 GHz to 23.12 GHz. According to Fig. 8(c), the average phase differences at the center frequency 22 GHz are −45.28°, 135.28°, −135.43°, and 45.13°, which are close to the expected values of −45°, 135°, −135°, and 45°. In Fig. 5(c), the frequency dependence of phase shift values for Assignment 5 has worse performance than for Assignment 1. In addition, the phase shifters used in Assignment 5 show narrower bandwidth and serious degradation especially at lower frequencies. Therefore, the phase difference flatness of Assignment 1 is as expected and better than the one of Assignment 5, as shown in Figs. 7(c) and 8(c).

Fig. 9(a) reports the array factor at the center frequency obtained using the complex amplitude at the four output ports and assuming an array spacing of $0.58\lambda_0$, where $\lambda_0$ is the free-space wavelength at 22 GHz. The scanning range in $\theta$ is from −90° to 90°. The input ports of Assignments 1 and 5 have different adjacent output phase differences, so the input ports being assigned with the same adjacent output phase differences are compared. For example, Port 2 in Assignment 1 is compared with Port 4 in Assignment 5, which have the same

**TABLE 7. Worst Case Deviation of Output Ports Amplitude From 21 GHz to 23 GHz (From 20.5 GHz to 23.5 GHz in Parentheses) (Unit: dB)**

| Assignment | Input Port 1 | Input Port 2 | Input Port 3 | Input Port 4 |
|---|---|---|---|---|
| 1 | −1.17 (−5.43) | −2.15 (−3.54) | −2.15 (−3.53) | −1.17 (−5.42) |
| 5 | −1.00 (−9.57) | −1.71 (−9.11) | −1.71 (−9.10) | −0.99 (−9.55) |

adjacent output phase difference of −45°. All the ports have nearly the same performance in terms of array factor pattern at the center frequency. Assignment 5 may have tiny differences on sidelobes compared with Assignment 1, but these are marginal. Fig. 9(b) shows the frequency dependence of the array factor at the peak directions for the two assignments with the same array spacing assumption. The peak direction is fixed for all frequencies and is determined by the one at 22 GHz. From these results, it is clear that Assignment 1 has a more stable performance over frequency, while Assignment 5 has serious degradation at the lower analyzed frequencies, mostly due to the poor performance of the phase shifters which causes the large reflections at the input ports and the greater imbalance among the four output ports. Especially, the imbalance of the adjacent output phase differences shown in Fig. 8(c) is significant. For the ±45° case, Assignment 1 shows good flatness over the frequency range from 21 GHz to 23.50 GHz. However, Assignment 5 has comparable performance to Assignment 1 only from 21.64 GHz to 22.56 GHz, and degrades seriously at frequencies below 21.64 GHz. Similarly, for the ±135° case, Assignment 1 shows much better stability, but Assignment 5 has stable performance only from 21.56 GHz to 22.52 GHz, and has significant degradation for frequencies below 21.56 GHz. At the center frequency, both assignments have the array factor peak value of 5.82 dBi when output phase differences are ±45° and 5.81 dBi when output phase differences are ±135°. These values are in line with the expected theoretical value of 6.02 dB, corresponding to the array factor of an ideal 1 × 4 linear array, the difference being the consequence of the small amplitude and phase errors at 22 GHz. Because the matrix designs are symmetric, only half of the array factors are reported.

To provide a comparison between the two switching matrices, worst case deviation figures are reported in amplitude and phase in Tables 7 and 8, respectively. These results are evaluated over the frequency range from 21 GHz to 23 GHz, corresponding approximately to the common range of operation of the two designs. The values in the parentheses are evaluated from 20.5 GHz to 23.5 GHz, highlighting further the differences between the two designs. Only the results for Input ports 1 and 2 are shown due to the symmetric structures. Table 7 shows the amplitude imbalance between output channels for both assignments. The deviation shows the error compared with the ideal value of −6.02 dB. The two designs have similar performance over the nominal bandwidth, while the difference is more significant over the extended bandwidth. Table 8 reports the phase stability of the two assignments. The worst case deviation of phase differences between Output ports 5 and 6 from 21 GHz to 23 GHz, and from 20.5 GHz to 23.5 GHz in parentheses, for the four input ports are given as examples. Assignment 1 shows clearly more stable phase differences than Assignment 5, even within the nominal frequency range. This result confirms the impact of the phase shift values on the overall matrix performance. Finally, Table 9 reports the insertion loss due to the conductor and dielectric for the two assignments. For this assessment, a conductivity of $5.8 \times 10^7$ S/m and a loss tangent of 0.00085 are included in the model, and the losses are evaluated comparing these results with those of the ideal model used as reference in this section. The worst case values of the insertion loss over the frequency ranges from 21 GHz to 23 GHz and 20.5 GHz to 23.5 GHz in parentheses are reported. Assignment 1 shows lower insertion loss than Assignment 5 in most cases, although the values remain comparable. The difference is attributed to the phase shifters which operate closer to the cut-off frequency, thus introducing slightly higher insertion losses.

**TABLE 8. Worst Case Deviation of Phase Differences Between Output Ports 5 and 6 From 21 GHz to 23 GHz (From 20.5 GHz to 23.5 GHz in Parentheses) (Unit: deg.)**

| Assignment | Input Port 1 | Input Port 2 | Input Port 3 | Input Port 4 |
|---|---|---|---|---|
| 1 | 2.58 (16.48) | 17.04 (22.78) | 8.10 (25.28) | 15.25 (30.00) |
| 5 | 106.85 (179.06) | 73.74 (121.37) | 12.82 (15.98) | 41.70 (66.48) |

**TABLE 9. Worst Case Insertion Loss for Assignments 1 and 5 From 21 GHz to 23 GHz (From 20.5 GHz to 23.5 GHz in Parentheses)**

| Assignment | Input Port | Output Port | Largest Insertion Loss (dB) |
|---|---|---|---|
| 1 / 5 | 1 | 5 | 0.62 / 0.91 (0.62 / 1.01) |
| 1 / 5 | 1 | 6 | 0.64 / 0.61 (0.81 / 0.63) |
| 1 / 5 | 1 | 7 | 0.60 / 0.63 (0.69 / 0.64) |
| 1 / 5 | 1 | 8 | 0.61 / 0.80 (0.66 / 0.87) |
| 1 / 5 | 2 | 5 | 0.61 / 0.81 (0.63 / 0.93) |
| 1 / 5 | 2 | 6 | 0.57 / 0.61 (0.65 / 0.69) |
| 1 / 5 | 2 | 7 | 0.62 / 0.70 (0.62 / 0.95) |
| 1 / 5 | 2 | 8 | 0.60 / 0.75 (0.65 / 0.91) |

### *D. EXPERIMENTAL VERIFICATION OF THE 4 × 4 MATRIX PROTOTYPES*

The full 4 × 4 matrices for two assignments are fabricated and measured. Fig. 10 shows photos of the two manufactured matrices, where the size of the substrate board is 296.78 mm × 112.00 mm × 3.20 mm. For the measurements, transitions from post-wall to standard waveguide are added to the two sides of the matrix. The eight transitions should have the same

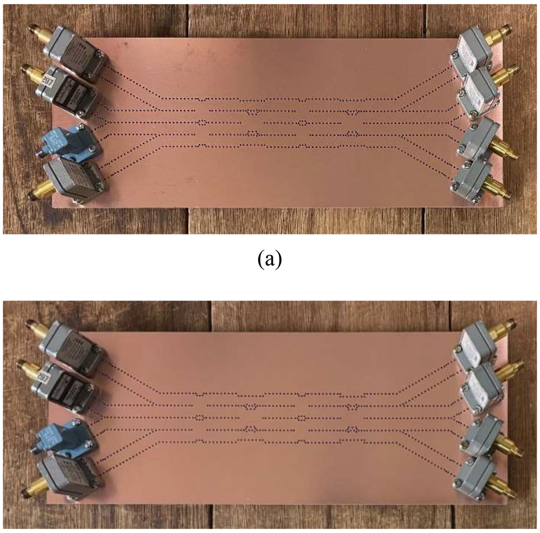

(a)

(b)

**FIGURE 10.** Photo of the two manufactured matrices, (a) assignment 1, and (b) assignment 5.

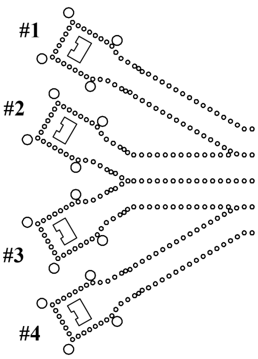


**FIGURE 11.** Structure of post-wall-to-waveguide transitions on one side of the matrix.

length in order to avoid the influence of the transitions on the phase shift for each path. The design of the transition is detailed in [10]. Fig. 11 shows the design of the post-wall-to-waveguide transitions on one side. The simulation results of the transmission coefficients and the reflection coefficients are reported in Fig. 12. The bandwidth with a reflection below −15 dB is 13.00%, from 20.47 GHz to 23.33 GHz. Standard WR42 coaxial-to-waveguide transitions are used for the measurements. Since the same transitions are added to both matrices, they do not affect the conclusions of the comparative study.

In Fig. 13(a) to (c), the simulated and the measured results in amplitude and the phase differences between adjacent output ports for all input ports are shown, respectively, for the matrix corresponding to Assignment 1. The dashed lines show the simulation results, and the solid lines show the measured results. For Input ports 1 and 4, the simulation result show that the reflection is below −15 dB over a bandwidth of 10.86%, from 20.79 GHz to 23.18 GHz. The measured results show a reflection below −13.42 dB over a bandwidth of 11.59%,

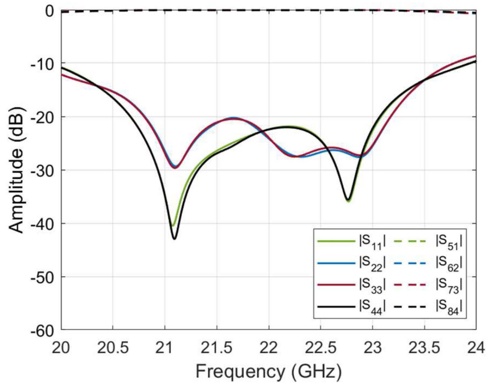


**FIGURE 12.** Simulation results of transitions on one side of the matrix (reflection coefficients in *solid lines* and transmission coefficients in *dashed lines*).

from 20.86 GHz to 23.41 GHz. The average transmission coefficients at the design frequency, 22 GHz, in simulation and measurement are −6.33 dB and −7.34 dB, respectively, indicating insertion losses in practice of about 1 dB. For Input ports 2 and 3, the simulation results show that the reflection is below −15 dB over a bandwidth of 12.05%, from 20.55 GHz to 23.20 GHz and very similar to the measured value of 12.36%, from 20.67 GHz to 23.39 GHz. The average transmission coefficients at 22 GHz in simulation and measurement are −6.37 dB and −7.42 dB. Fig. 13(c) plots phase differences between adjacent output ports. The average phase differences at the center frequency are −135.14°, 44.87°, −45.26°, and 134.78° for the simulation results, and −133.68°, 45.95°, −43.55°, and 137.58° for the measured results, compared with the expected values of −135°, 45°, −45°, and 135°.

Fig. 14(a) and (b) show the simulated and the measured results in amplitude and the phase differences between adjacent output ports for all input ports, respectively, for the matrix corresponding to Assignment 5. The simulation results are shown in dashed lines, and the measured results are shown in solid lines. For Input ports 1 and 4, the simulation result shows that the reflection is below −15 dB over a bandwidth of 9.50%, from 21.17 GHz to 23.26 GHz. The reflection in measurements is below −15 dB over a bandwidth of 9.77%, from 21.26 GHz to 23.41 GHz. The average transmission coefficients at 22 GHz in simulation and measurement are −6.36 dB and −7.46 dB, respectively, indicating insertion losses of about 1 dB. In the case of Input ports 2 and 3, the simulation results provide a reflection below −15 dB over a bandwidth of 7.91%, from 21.29 GHz to 23.03 GHz. Similar results are obtained in measurements, with a reflection below −15 dB over a bandwidth of 8.05%, from 21.47 GHz to 23.24 GHz. The average transmission coefficients at 22 GHz are −6.39 dB and −7.47 dB in simulation and measurement, respectively. In Fig. 14(c), phase differences between adjacent output ports are shown. The average phase differences at the center frequency are −44.87°, 135.90°, −135.26°, and 45.51° for the simulation results, and −47.19°, 133.89°, −134.05°,

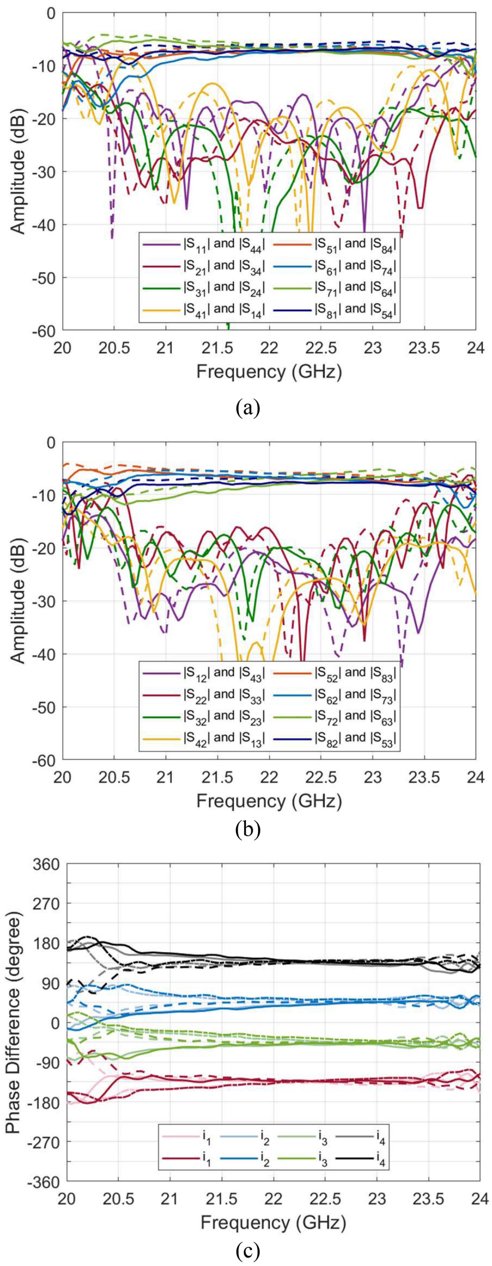


**FIGURE 13.** Simulated and Measured results for assignment 1 of the 4 × 4 parallel switching matrix with transitions: (a) and (b) amplitude in dB (simulation results in *dashed lines*, and measured results in *solid lines*), and (c) phase difference between adjacent ports in degree (between port 6 and port 5 in *solid lines*, between port 7 and port 6 in *dashed lines*, and between port 8 and port 7 in *dashed-dotted lines*; simulation results in *light colors*, and measured results in *dark colors*).

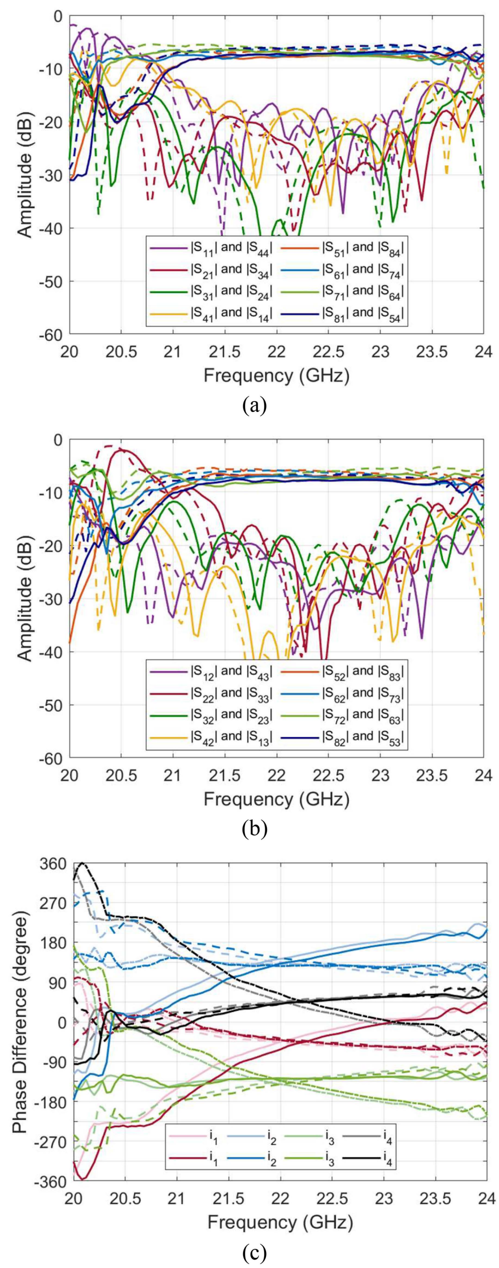


**FIGURE 14.** Simulated and Measured results for assignment 5 of the 4 × 4 parallel switching matrix with transitions: (a) and (b) amplitude in dB (simulation results in *dashed lines*, and measured results in *solid lines*), and (c) phase difference between adjacent ports in degree (between Port 6 and Port 5 in *solid lines*, between port 7 and port 6 in *dashed lines*, and between port 8 and port 7 in *dashed-dotted lines*; simulation results in *light colors*, and measured results in *dark colors*).

and 47.88° for the measured results, compared with the expected theoretical values of −135°, 45°, −45°, and 135°. The frequency dependence of the array factor at peak directions, which are fixed values obtained at 22 GHz, is reported in Fig. 15 for the two assignments. For the simulation results, the values at the center frequency are 5.66 dBi and 5.71 dBi for the phase differences ±45° and ±135° in the case of Assignment 1, and are 5.69 dBi and 5.65 dBi for the phase differences ±45° and ±135° in the case of Assignment 5. For the measurement results, the peak array factor of Assignment 1 is 4.61 dBi and 4.74 dBi for the output phase differences ±45° and ±135°, and 4.54 dBi and 4.57 dBi for Assignment 5 in the cases ±45° and ±135° respectively at 22 GHz. The difference between simulation and measurement is around 1 dB in all cases, which is slightly higher than the losses evaluated in Section III-C. This is because the results reported

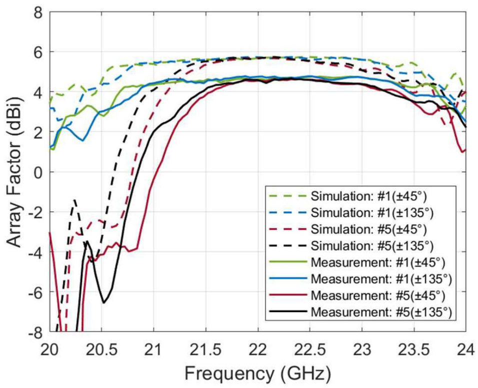


**FIGURE 15.** Frequency dependence of the array factor at peak directions for assignments 1 and 5 with transitions (simulation results in *dashed lines*, and measured results in *solid lines*).

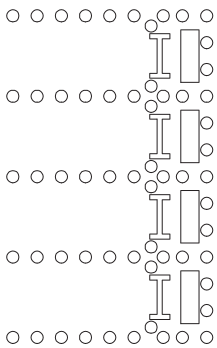

**FIGURE 16.** Structure of the 1 × 4 linear array.

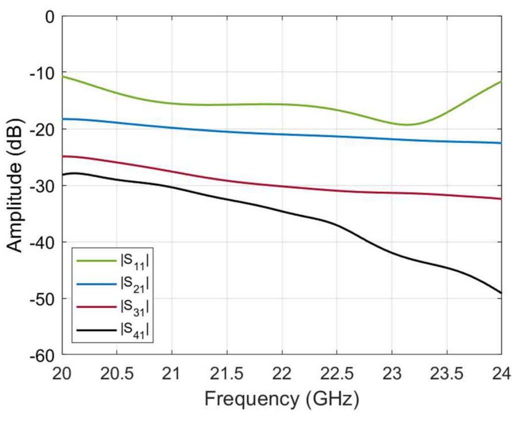


**FIGURE 17.** Simulation results of the 1 × 4 linear array, including reflection and isolation.

here also account for the losses of the transitions. In operation, those transitions will not be present, so the actual losses of the matrices are expected to be lower. Similar to the simulation results of the full matrix without transitions mentioned in the previous section, Assignment 1 shows stable performance over the reported frequency range, while Assignment 5 shows significant degradation in the lower range of the analyzed frequency band due to the large reflection and the dispersion among output ports for both the simulated and the measured results. Although less significant, the peak array factor values

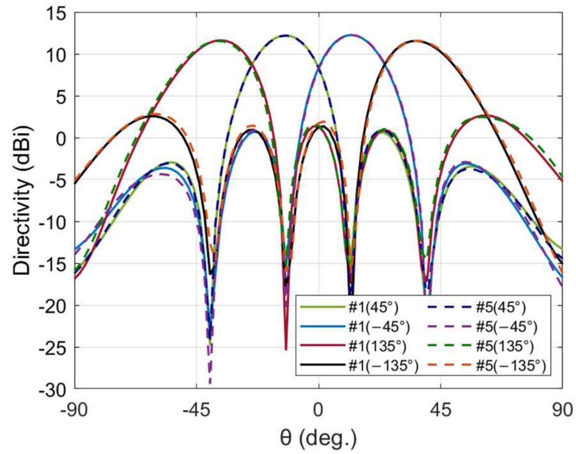


**FIGURE 18.** Radiation patterns of the 1×4 linear array fed by the 4×4 switching matrices with assignments 1 and 5 at 22 GHz.

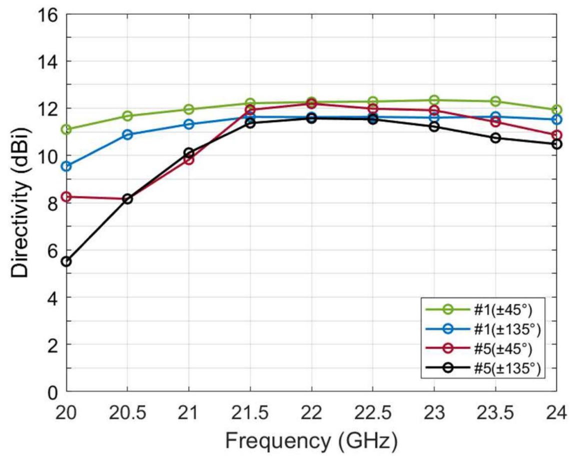


**FIGURE 19.** Frequency dependence of the directivity of the beams radiated by the 1×4 linear array fed by the 4×4 switching matrices with assignments 1 and 5.

of Assignment 5 are also below those of Assignment 1 in the upper frequency range, due to the larger phase errors as reported in Fig. 14(c). These results confirm experimentally that the standard Butler matrix design is not necessarily the optimal implementation in a single-layer PCB design, and other output phase difference assignments are found more advantageous when accounting for the impact of the crossovers and imposing restrictions on the envelop of the matrix.

### *E. VERIFICATION OF THE RADIATING PERFORMANCE OF THE 4 × 4 MATRIX PROTOTYPES*

The full 4 × 4 matrices for the two assignments are combined with a 1 × 4 linear array to verify their radiating performance. Fig. 16 shows the design of the linear array. It has an "H" slot, a "rectangular" slot, and two reflection canceling posts in order to achieve a wider bandwidth [30]. The simulated S-parameters of the linear array are reported in Fig. 17. The reflection coefficient is below −15 dB over a bandwidth of 13.23%, from 20.78 GHz to 23.69 GHz, and below −10 dB over a bandwidth of 18.18%, thus not limiting the frequency bandwidth of the matrices.

By combining the simulated 1 × 4 linear array with the S-parameters of the matrices, more accurate radiating performance can be reported. Fig. 18 shows the radiation patterns at the center frequency, which combine the array factor and elementary patterns. According to the assignment of adjacent output phase differences, Ports 2, 3, 4, and 1 in Assignment 1 correspond to Ports 4, 1, 2, and 3 in Assignment 5, which have the phase differences of 45°, −45°, 135°, and −135° respectively. The results of Assignment 5 show a good match with the ones of Assignment 1 since Assignment 5 does not have much degradation at the center frequency. The frequency dependence of the radiating properties is also investigated, which is reported in Fig. 19. It shows the peak values of radiation patterns over the analyzed frequency band. Due to the symmetric structures, only half of the results are reported for the two assignments. Assignment 5 does have similar results to Assignment 1 when the frequency is close to the center frequency; however, it has much lower directivity at lower frequencies, as expected from the matrix results in the previous section. The beams with ±135° output phase differences show lower values than the ones with ±45° output phase difference from 20 GHz to 22 GHz since a larger tilting angle leads to higher scan loss introduced by the element pattern.

## IV. CONCLUSION

A special configuration of 1-D parallel switching matrices with four beams realized in post-wall waveguide technology has been discussed in this article. The matrices use PTFE as substrate and the design frequency is 22 GHz. Two special output phase difference assignments, referred to as Assignment 1, having the smallest phase difference with reference to the transmission phase of a straight waveguide with the same length as the coupled region of the crossover, and Assignment 5, the well-known conventional Butler matrix configuration, have been selected for a detailed comparative study. The full matrices without transitions, the ones with transitions, and the ones combined with a linear array have been analyzed. The ones with transitions have been fabricated and measured. Ideal results of transmission coefficients, reflection coefficients, and phase differences have been obtained in all cases. The simulation results and the measured results of the matrices with transitions are in good agreement. As expected, the matrices with transitions have slightly degraded performance than the ones without transitions, but the bandwidth characteristics are preserved. These results confirm that planar implementations using crossover couplers may be improved carefully selecting the output phase assignment, as the one corresponding to the conventional Butler matrix configuration is not necessarily the optimal one. The special configuration of 1-D parallel switching matrices with other numbers of beams will be investigated in the future.

## REFERENCES


[1] T. Chaloun et al., "Electronically steerable antennas for future heterogeneous communication networks: Review and perspectives," *IEEE J. Microwaves*, vol. 2, no. 4, pp. 545–581, Oct. 2022.

[2] Y. J. Guo, M. Ansari, and N. J. G. Fonseca, "Circuit type multiple beamforming networks for antenna arrays in 5G and 6G terrestrial and non-terrestrial networks," *IEEE J. Microwaves*, vol. 1, no. 3, pp. 704–722, Jul. 2021, doi: 10.1109/jmw.2021.3072873.

[3] P. Angeletti and M. Lisi, "Multimode beamforming networks for space applications," *IEEE Antennas Propag. Mag.*, vol. 56, no. 1, pp. 62–78, Feb. 2014.

[4] G. Amendola et al., "Low-Earth orbit user segment in the Ku and Ka-band: An overview of antennas and RF front-end technologies," *IEEE Microwaves Mag.*, vol. 24, no. 2, pp. 32–48, Feb. 2023.

[5] J. Blass, "The multidimensional antenna: A new approach to stacked beams," *IRE Int. Conv. Rec. 1*, vol. 8, pp. 48–50, Mar. 1960.

[6] S. Mosca, F. Bilotti, A. Toscano, and L. Vegni, "A novel design method for Blass matrix beam-forming networks," *IEEE Trans. Antennas Propag.*, vol. 50, no. 2, pp. 225–232, Feb. 2002.

[7] J. Butler and R. Lowe, "Beam forming matrix simplifies design of electronically scanned antenna," *Electron. Des.*, vol. 9, no. 8, pp. 170–173, Apr. 1961.

[8] S. Yamamoto, J. Hirokawa, and M. Ando, "A beam switching slot array with a 4-way Butler matrix installed in a single layer post-wall waveguide," in *Proc. IEEE Antennas Propag. Soc. Int. Symp.*, 2002, pp. 138–141, doi: 10.1109/APS.2002.1016269.

[9] A. A. M. Ali, N. J. G. Fonseca, F. Coccetti, and H. Aubert, "Design and implementation of two-layer compact wideband Butler matrices in SIW technology for Ku-band applications," *IEEE Trans. Antennas Propag.*, vol. 59, no. 2, pp. 503–512, Feb. 2011.

[10] T. Djerafi and K. Wu, "A low-cost wideband 77-GHz planar Butler matrix in SIW technology," *IEEE Trans. Antennas Propag.*, vol. 60, no. 10, pp. 4949–4954, Oct. 2012.

[11] J. Nolen, "Synthesis of multiple beam networks for arbitrary illuminations," Ph.D. dissertation, Bendix Corp., Radio Div., Baltimore, MD, USA, Apr. 1965.

[12] N. J. G. Fonseca, "Printed S-band 4x4 Nolen matrix for multiple beam antenna applications," *IEEE Trans. Antennas Propag.*, vol. 57, no. 6, pp. 1673–1678, Jun. 2009.

[13] P. Li, H. Ren, and B. Arigong, "A symmetric beam-phased array fed by a Nolen matrix using 180° couplers," *IEEE Microwaves Wireless Compon. Lett.*, vol. 30, no. 4, pp. 387–390, Apr. 2020.

[14] W. White, "Pattern limitations in multiple-beam antennas," *IRE Trans. Antennas Propag.*, vol. 10, no. 4, pp. 430–436, 1962.

[15] N. J. G. Fonseca, "Discussion on reciprocity, unitary matrix, and lossless multiple beam forming networks," *Int. J. Antennas Propag.*, vol. 2015, pp. 1–9, Apr. 2015.

[16] J. P. Shelton and K. S. Kelleher, "Multiple beams from linear arrays," *IRE Trans. Antennas Propag.*, vol. 9, no. 2, pp. 154–161, Mar. 1961, doi: 10.1109/tap.1961.1144964.

[17] K. Han, G. Wei, S. Lei, M. Wang, and T. Qiu, "Design of broadband 9 × 9 Butler matrix and its extension for multibeam application," *IEEE Trans. Circuits Syst. II, Exp. Briefs*, early access, Mar. 03, 2023, doi: 10.1109/TCSII.2023.3252527.

[18] J. P. Shelton, "Fast Fourier transforms and Butler matrices," *Proc. IEEE*, vol. 56, no. 3, pp. 350–350, Mar. 1968.

[19] W. Nester, "The fast Fourier transform and the Butler matrix," *IEEE Trans. Antennas Propag.*, vol. 16, no. 3, pp. 360–360, May 1968.

[20] T. Djerafi, N. J. G. Fonseca, and K. Wu, "Broadband substrate integrated waveguide 4 × 4 Nolen matrix based on coupler delay compensation," *IEEE Trans. Microwaves Theory Techn.*, vol. 59, no. 7, pp. 1740–1745, Jul. 2011.

[21] J. Hirokawa and N. J. G. Fonseca, "Generalized one-dimensional parallel switching matrices with an arbitrary number of beams," *IEEE J. Microwaves*, vol. 1, no. 4, pp. 975–988, Oct. 2021.

[22] T. Kai, J. Hirokawa, and M. Ando, "Feed through an aperture to a post-wall waveguide with step structure," *IEICE Trans. Commun.*, vol. E88-B, no. 3, pp. 1298–1302, Mar. 2005.

[23] K. Wu, M. Bozzi, and N. J. G. Fonseca, "Substrate integrated transmission lines: Review and applications," *IEEE J. Microwaves*, vol. 1, no. 1, pp. 345–363, Jan. 2021.

[24] J. Hirokawa and N. J. G. Fonseca, "Special assignments of adjacent output phase differences per input ports in generalized one-dimensional parallel switching matrices," *IEICE Commun. Exp.*, vol. 11, no. 6, pp. 268–272, Jun. 2022.

[25] T. Djerafi, N. J. G. Fonseca, and K. Wu, "Design and implementation of a planar 4x4 Butler matrix in SIW technology for wide band high power applications," *Prog. Electromagn. Res. B*, vol. 35, pp. 29–51, Oct. 2011.

[26] Q.-L. Yang, Y.-L. Ban, K. Kang, C.-Y. -D. Sim, and G. Wu, “SIW multibeam array for 5G mobile devices,” *IEEE Access*, vol. 4, pp. 2788–2796, 2016.

[27] Q. Sun, Y.-L. Ban, Y.-X. Che, and Z. Nie, “Coexistence-mode CRLH SIW transmission line and its application for longitudinal miniaturized Butler matrix and multibeam array antenna,” *IEEE Trans. Antennas Propag.*, vol. 69, no. 11, pp. 7593–7603, Nov. 2021.

[28] Y. Zhu and C. Deng, “Millimeter-wave dual-polarized multibeam endfire antenna array with a small ground clearance,” *IEEE Trans. Antennas Propag.*, vol. 70, no. 1, pp. 756–761, Jan. 2022.

[29] W. Kahn and H. Kurss, “The uniqueness of the lossless feed network for a multibeam array,” *IRE Trans. Antennas Propag.*, vol. 10, no. 1, pp. 100–101, Jan. 1962.

[30] Z. Zou, Y. Ding, G. Zhu, Y. Li, and G. Yang, “Broadband SIW slot antenna for millimeter wave application,” in *Proc. IEEE Int. Symp. Antennas Propag.*, 2021, pp. 641–642, doi: 10.23919/ISAP4705-3.2021.9391267.

**SHENGJIA WU** (Student Member, IEEE) was born in Nagoya, Japan, in 1998. She received the B.S. degree in electrical engineering from the University of California, Davis, Davis, CA, USA, in 2020. She is currently working toward the M.S. degree in electrical and electronic engineering with the Tokyo Institute of Technology, Tokyo, Japan. Her research focuses on one-dimensional parallel switching matrices.

**JIRO HIROKAWA** (Fellow, IEEE) was born in Tokyo, Japan, in 1965. He received the B.S., M.S., and D.E. degrees in electrical and electronic engineering from the Tokyo Institute of Technology (Tokyo Tech), Tokyo, Japan, in 1988, 1990, and 1994, respectively. He was a Research Associate from 1990 to 1996 and an Associate Professor from 1996 to 2015 with Tokyo Tech. He is currently a Professor with Tokyo Tech. From 1994 to 1995, he was a Postdoctoral Fellow with the Antenna Group of Chalmers University of Technology, Gothenburg, Sweden. He has authored or co-authored more than 200 peer-reviewed journal papers and more than 600 international conference presentations. His research interests include analyses, designs, and fabrication techniques of slotted waveguide array antennas, millimeter-wave, and terahertz antennas, and beam-switching circuits. He was an Associate Editor for *IEICE Transactions on Communications* during 1999–2003 and 2004–2007. He was also an Associate Editor during 2013–2016, and the Track Editor during 2016–2022 for IEEE TRANSACTIONS ON ANTENNAS AND PROPAGATIONS. Since 2023, he has been the Track Editor for IEEE ANTENNAS AND WIRELESS PROPAGATION LETTERS. He was the Chair of the Technical Program Committee for ISAP 2016. From 2017 to 2019, he was also the Chair of IEICE Technical Committee on Antennas and Propagation. He was the recipient of IEEE AP-S Tokyo Chapter Young Engineer Award in 1991, Young Engineer Award from IEICE in 1996, Tokyo Tech Award for Challenging Research in 2003, Young Scientists’ Prize from the Minister of Education, Cultures, Sports, Science and Technology in Japan, in 2005, Best Paper Award in 2007 and a Best Letter Award in 2009 from IEICE Communications Society, and IEICE Best Paper Award in 2016 and 2018. He is a Fellow of IEICE.

**TAKASHI TOMURA** (Member, IEEE) received the B.E., M.E., and D.E. degrees in electrical and electronic engineering from Tokyo Institute of Technology, Tokyo, Japan, in 2008, 2011, and 2014, respectively. In 2013, he was a Research Fellow of the Japan Society for the Promotion of Science. From 2014 to 2017, he was with Mitsubishi Electric Corporation, Tokyo, and was engaged in research and development of aperture antennas for satellite communications and radar systems. From 2017 to 2019, he was a specially appointed Assistant Professor with Tokyo Institute of Technology. He is currently an Assistant Professor with Tokyo Institute of Technology. His research interests include electromagnetic analysis, aperture, reflectarray, and waveguide slot array antennas. Dr. Tomura was the recipient of the Best Student Award from Ericsson Japan in 2012, IEEE AP-S Tokyo Chapter Young Engineer Award in 2015, Young Researcher Award from IEICE Technical Committee on Antennas and Propagation in 2018, and IEEE MTT-S Japan Chapter Young Engineer Award in 2022. He is a member of IEICE.

**NELSON J. G. FONSECA** (Senior Member, IEEE) received the M.Eng. degree in electrical engineering from the Ecole Nationale Superieure d’Electrotechnique, Electronique, Informatique, Hydraulique et telecommunications (ENSEEIHT), Toulouse, France, in 2003, the M.Sc. degree in electrical engineering from the Ecole Polytechnique de Montreal, Montreal, QC, Canada, in 2003, and the Ph.D. degree in electrical engineering from Institut National Polytechnique de Toulouse - Universite de Toulouse, Toulouse, in 2010. He is currently an Antenna Engineer with the Antenna and Sub-Millimetre Waves Section, European Space Agency, Noordwijk, The Netherlands. Since November 2020, he has been an Honorary Professional Fellow with the University of Technology Sydney, Sydney, NSW, Australia. He has authored or coauthored more than 300 papers in peer-reviewed journals and conferences and has more than 50 patents issued or pending. His research interests include multiple beam antennas for space missions, beamformer theory and design, ground terminal antennas, transfer of technology from and to terrestrial systems, including 5G networks, and novel manufacturing techniques. Dr. Fonseca is currently an Associate Editor for IEEE TRANSACTIONS ON ANTENNAS AND PROPAGATIONS and *IET Microwaves, Antennas and Propagation*. He is also a Topic Editor for JOURNAL OF MICROWAVES. He is the Chair of the newly founded IEEE MTT-S Technical Committee 29 on Microwave Aerospace Systems. Since January 2019, he has been a Board Member of the European School of Antennas and Propagation (ESoA) and also the coordinator of the ESA/ESoA course on Antennas for Space Applications, for which he was voted best Lecturer by the participants of the 2020 edition. He is the elected EurAAP Regional Delegate representing Benelux for the term 2021-2023.